Temperature dependent non-monotonic bands shift in $ZrTe_5$

G. Manzoni [a], A. Crepaldi [b,c], G. Autès [c,d], A. Sterzi [a], F. Cilento [b], A. Akrap [e], I. Vobornik [f], L. Gragnaniello [g], Ph. Bugnon [c], M. Fonin [g], H. Berger [c], M. Zacchigna [f], O.V. Yazyev [c,d], F. Parmigiani [a,b,h,*]

[a] *Universitá degli Studi di Trieste, Via A. Valerio 2, Trieste 34127, Italy*
[b] *Elettra – Sincrotrone Trieste S.C.p.A., Strada Statale 14, km 163.5, Trieste, Italy*
[c] *Institue of Physics, Ecole Polytechnique Fédérale de Lausanne (EPFL), CH-1015 Lausanne, Switzerland*
[d] *National Centre for Computational Design and Discovery of Novel Materials MARVEL, Ecole Polytechnique Fédérale de Lausanne (EPFL), CH-1015 Lausanne, Switzerland*
[e] *DQMP, University of Geneva, CH-1211 Geneva 4, Switzerland*
[f] *CNR-IOM, Strada Statale 14, km 163.5, 34149 Trieste, Italy*
[g] *University of Konstanz, 78457 Konstanz, Germany*
[h] *International Faculty, University of Köln, 50937 Köln, Germany*

A B S T R A C T

The electronic structure of $ZrTe_5$ has been matter of renewed interest aimed at clarifying, along with its topological character, the temperature dependence of the unusual transport properties of this material. Here, we report an extensive high resolution Angle Resolved Photoelectron Spectroscopy (ARPES) study unveiling a non-monotonic shift of the bands, when the sample temperature is varied between 16 K and 300 K. Moreover, the present conventional ARPES and circularly dichroic ARPES measurements reveal the presence of two states at the top of the valence band. The strong ARPES dichroic signal detected in proximity of the Fermi energy has been interpreted as the indication of the presence of spin polarized states, in agreement with the predicted strong topological character of this material.

1. Introduction

The recent debate about the topological character of $ZrTe_5$ [1–6] has triggered novel studies aimed at understanding the origins of its exotic transport properties [7–9].

The unusual temperature evolution of the electronic transport properties of $ZrTe_5$ consists in a resisitivity peak at T^* accompanied by a sign reversal of the Seebeck coefficient. However, due to the presence of impurities and defects deriving from the sample growth conditions [10,11], T^* is strongly sample dependent and it can vary from ∼60 K to ∼170 K [1,7,12,13].

The origin of these anomalous properties has been subject of debate and different mechanisms including a structural phase transition [11,14], formation of charge density waves (CDW) [7,15] and the presence of polaronic charge carriers [10] have been considered. However, direct experimental evidences supporting these theories are still lacking [11,15], and an unanimous consensus about the band structure behaviour versus temperature has not been reached.

Our previous band structure investigation [16] has revealed a band shift towards lower $E - E_F$ energies, which was monotonic in the investigated temperature range of 300–125 K. In particular, the binding energy of the characteristic Dirac cone at the Γ point of the Brillouin zone reaches its maximum at ∼T^* [16].

Recent ARPES data [12], performed between ∼300 K and ∼2 K, have shown that the band shift is monotonic toward higher binding energies, when the sample is cooled. As a consequence, the Dirac point and the bottom of the conduction band (CB) are detected below the Fermi energy (E_F) at ∼2 K [12]. Conversely, other ARPES experiments, done at 24 K [5] and at 20 K [1], have shown the Bulk
Valence Band (BVB) of $ZrTe_5$ crossing E_F.

In this work, we have performed Angle Resolved Photoelec-tron Spectroscopy (ARPES) measurements in a temperature range between 16 K and 300 K, revealing a non-monotonic band shift across the Fermi level at $k_a = k_c = 0$ Å, with the inversion point in proximity of T^*. The shift of the Dirac point across E_F seems to be consistent with the resistivity peak detected at T^*, as we have reported in our previous study [16]. However, the discovery of a

* Corresponding author at: Universitá degli Studi di Trieste, Via A. Valerio 2, Trieste 34127, Italy.

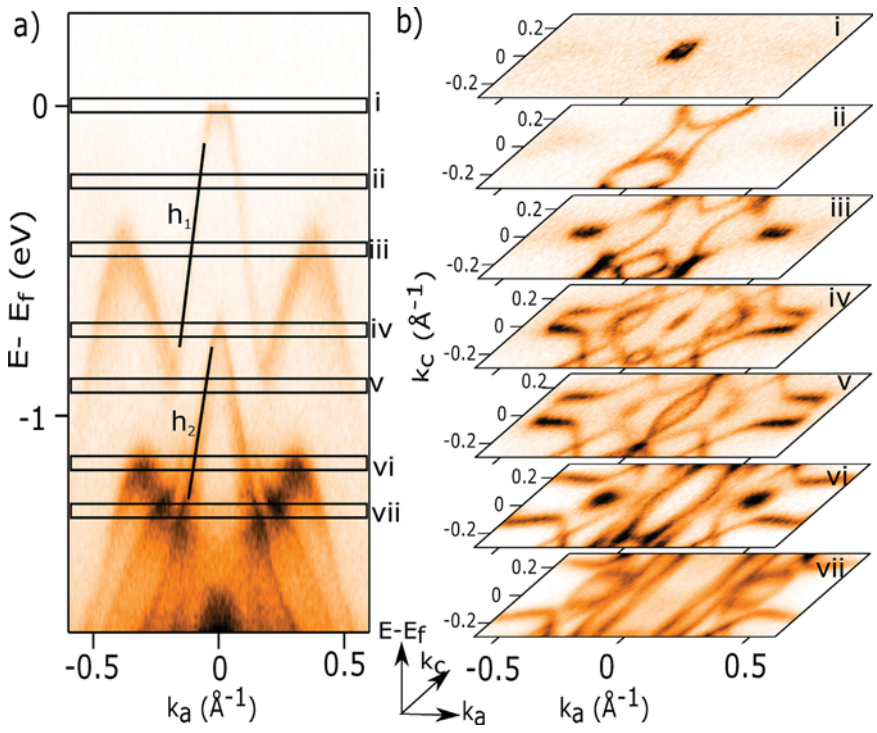

Fig. 1. (a) Electronic band structure of $ZrTe_5$ along the k_a direction measured at ~16 K with photon energy of 22 eV. The black lines, h_1 and h_2, indicate two bands dispersing with similar group velocity: $V_{h_1} \sim 8 \pm 1 \times 10^5$ m/s and $V_{h_2} \sim 7 \pm 1 \times 10^5$ m/s. (b) Constant energy maps obtained integrating ~45 meV around (i) E_F, (ii) −0.24 eV, (iii) −0.46 eV, (iv) −0.72 eV, (v) −0.88 eV, (vi) 1.15 eV and (vii) −1.30 eV.

non-monotonic behaviour of the energy band shift calls for a different explanation than what we have reported before [16] about the carrier sign change, as we will further discuss in the following. Depending on the crystal lattice parameters, theoretical calculations have predicted $ZrTe_5$ to be at the verge of a topological phase transition between strong and weak topological insulator (STI-WTI) [3]. Scanning tunneling microscopy/spectroscopy (STM/STS) experiments have proposed the existence of unidimensional topologically protected states at step edges [4,5], suggesting the possibility that the material is in the WTI phase. The prediction of the STI phase of $ZrTe_5$ has been also recently supported by a combined ARPES and STM/STS study [6].

In order to better clarify the topological phase of $ZrTe_5$, the STI character of this material is discussed here in the light of high resolution (HR) ARPES data and circular dichroic (CD) ARPES measurements. In particular, the strong CD signal observed in proximity of the Fermi energy is proposed to be a fingerprint of the presence of spin polarized states. This supports the STI nature of $ZrTe_5$.

2. Methods

High quality $ZrTe_5$ single crystals have been grown by vapor transport technique with iodine methods [17]. $ZrTe_5$ presents an orthorombic structure and belongs to the *Cmcm* (D_{2h}^{17}) point group symmetry. Prismatic $ZrTe_3$ chains are connected by Te atoms along the *c* axis, with *a* = 3.99Å and *c* = 13.73Å as determined by X-ray powder diffraction [18]. Each crystal cell contains two $ZrTe_5$ planes piled along the *b* axis, with an interlayer distance, at 300 K, of 7.23 Å as determined by previous XRD study. The planes are weakly bounded by van der Waals forces. The clean surface exposed after a cleave is the $a - c$ surface.

ARPES measurements have been carried out at the APE beamline, Elettra, with linear horizontal (LH) polarization at a fixed photon energy of 22 eV. Valence bands and Fermi surface measurements were performed using a high resolution VG-SCIENTA DA30 electron analyzer, with energy and angular resolution better than 20 meV and 0.2°, respectively. The VG-SCIENTA DA30 electron analyzer has the capability to map the momentum space in two dimensions, k_a and k_c, without moving the sample. In our case, k_a was along the slit direction, k_c was scanned via the newly developed deflector system. Samples have been cleaved in ultrahigh vacuum (UHV, base pressure $p \sim 1 \times 10^{-10}$ mbar) at room temperature and mounted on a variable temperature cryostat; data have been collected from 16 K to 300 K. The crystals have been previously oriented by low-energy electron diffraction (LEED).

The resistivity was determined using four-point method, with the contacts made using silver paste and gold wires. The current was injected along the *a* axis. The measured samples were several mm long.

Density functional theory (DFT) calculations of bulk $ZrTe_5$ electronic structure were performed within the generalized gradient approximation as implemented in the Quantum-Espresso package [19]. Spin–orbit coupling (SOC) is taken into account with the help of fully relativistic norm-conserving pseudopotentials. The calculations were carried out using an $24 \times 24 \times 12$ *k*-point mesh and a planewave kinetic energy cutoff of 80 Ry for the wavefunctions. We used the experimentally determined crystal structure from Ref. [18].

3. Results

3.1. $ZrTe_5$ band structure at 16 K

Fig. 1 shows the results of high resolution ARPES measurement along the k_a direction (panel (a)) and different constant energy maps in the $k_a - k_c$ plane (panel (b)), as obtained by integrating over ~45 meV at selected binding energies. The sample tempera-ture was ~16 K. The $ZrTe_5$ Fermi surface is shown in panel (b–i). The hole-like state h_1 forms a circular pocket at E_F, and its evolution is tracked in Fig. 1(b-i)–(b-iv). The pocket changes from a circle to a

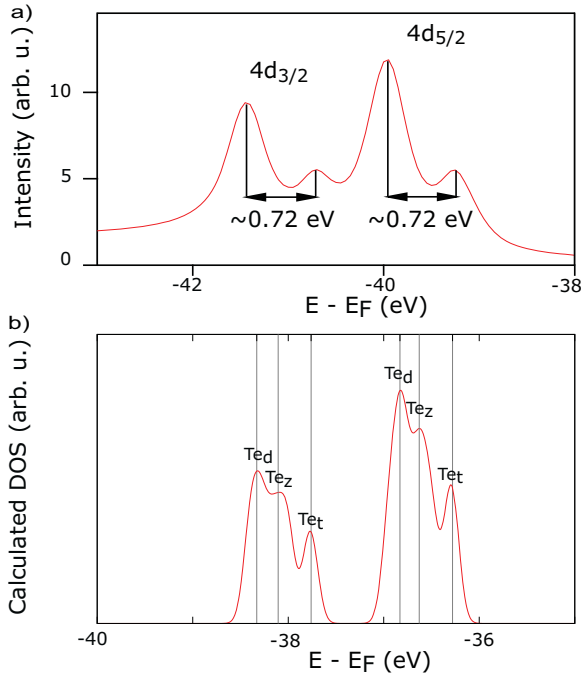

Fig. 2. (a) Measured Te core levels: $4d_{3/2}$ and $4d_{5/2}$. (b) Calculated Te 4*d* core levels.

warped rectangle (b-i)–(b-ii), then, it evolves in a more complex shape (Fig. 1(b-iii)–(b-iv)).

Fig. 1(a) reveals another band, h_2, dispersing with similar group velocity of h_1 and appearing at higher binding energy. This band (see Fig. 1(a)) has the maximum located at $k_a = k_c \simeq 0\text{Å}^{-1}$ and binding energy ~−0.72 eV. The bands velocities V_{h_1} and V_{h_2} have been estimated $\sim 8 \pm 1 \times 10^5$ m/s and $\sim 7 \pm 1 \times 10^5$ m/s, respectively.

The different evolutions of the two bands in the constant energy maps (CEMs) of Fig. 1(b) have given the possibility to discard the idea, suggested by the close V_{h_1} and V_{h_2} values, that h_2 might be a higher binding energy replica of h_1, as reported for other compounds having multiple surface terminations [20]. In particular, Fig. 1(b-v) shows that h_2 does not evolve in a warped rectangle, as h_1 in panel (b-ii), but in an almond-like shape, suggesting a different origin for the h_1 and h_2 bands. Moreover, in (b-vi) and (b-vii), the quasi 1D character of h_2 is revealed by the linear dispersion of the band that crosses the surface Brillouin zone (BZ) with negligible dispersion along the k_c direction. This observation provides new information about this material. Indeed, even though the crystal is formed by chains with reduced dimensionality, the quasi 1D band h_2 does not reach E_F. This can justify why the electronic transport properties reflect the two-dimensional character of h_1.

Another interesting feature of the $ZrTe_5$ electronic properties is the splitting of the $4d_{3/2}$ and $4d_{5/2}$ Te core levels. The Te 4*d* emission peaks, collected at a temperature of ~77 K and at pho-ton energy $h\nu = 75$ eV, are shown in Fig. 2(a). These spectra clearly show a replica shifted by ~0.72 eV for both the $4d_{3/2}$ and $4d_{5/2}$ spin–orbit splitted peaks. We ascribe this replica to the presence of two differently coordinated Te ions at the surface termination.

To better clarify the origin of these spectral features in the 4*d* core levels, we performed density functional theory (DFT) calculations. The calculated Te core levels are shown in Fig. 2(b).

Relativistic norm-conserving pseudopotentials were used, including the 4*d* core states for Te. The density of states projected on the 4*d* orbitals of the three types of Te atoms are shown in Fig. 2(b), where Te_t and Te_d correspond to the top and the two bottom atoms of the $ZrTe_3$ prism, while Te_z corresponds to the atoms connecting the $ZrTe_3$ chains along the *c* axis. As it can be seen, the

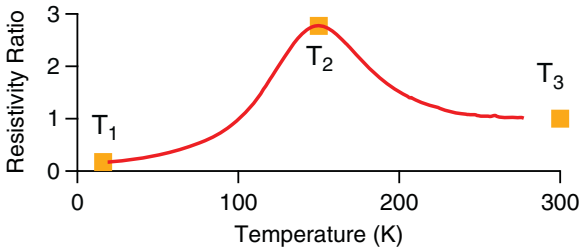

Fig. 3. (a) Normalized resitivity of $ZrTe_5$ as a function of temperature.

DFT results reproduce accurately the spin–orbit splitting of the 4*d* Te states. The splitting of the core levels of different sites, seen in experiment, is also qualitatively described. In particular, the Te_t core level are shifted up by ~0.6 eV with respect to the Te_z sites core level. The projected density of states, which relies on the position of Kohn–Sham eigenvalues and considers only the initial state, can just reproduce qualitatively the photoemission spectra. As a consequence, small discrepancies are observed in the energy shift estimation (~0.72 eV in the experiment, ~0.6 eV in the DFT model) and more importantly in the obtained binding energy values. However, the calculations provide us with valuable information about the mechanism at the origin of the chemical shift.

The calculated core level splitting gives an energetic position of the Te_z peaks which have not been observed experimentally. Within DFT, a more accurate estimation of the XPS spectra can be obtained by following the method proposed in Ref. [21]. Within this scheme, the core level shifts are calculated as the difference of total energy between the unexcited system and a system with a core hole on an excited Te atom. To simulate excited Te atoms, we produce a pseu-dopotential for Te with a hole in the 4*d* shell treated as a core level. One excited atom is then introduced as an impurity in a $2 \times 2 \times 2$ supercell for each of the three inequivalent Te positions. These cal-culations show, in agreement with the experiments, that the Te_d and Te_z core levels are separated by only ~8 meV while the Te_t core level is shifted upward by ~515 meV with respect to the Te_d level. The strong chemical shift of the Te_t core level with respect to the other Te sites can be ascribed to the different coordination of the Te ions. In particular, the Te_t atom at the top of the $ZrTe_3$ prism has longer bounds with the neighboring Zr and Te atoms when compared to the two other sites.

3.2. Temperature dependent non-monotonic bands shift

Having detailed the dispersion of some significative features of the $ZrTe_5$ band structure at ~16 K, we can now look at the evolution of the electronic properties with the temperature. This study is motivated by the anomalous resistivity peak (Fig. 3) reported vary-ing the sample temperature. For the sample used in the present experiment, the resistivity peak is located at $T^* \simeq 150$ K, but mea-surements carried out on different samples from the same batch, i.e. grown under the same conditions, reveal that T^* can vary from 140 K to 160 K.

We have investigated in details the temperature evolution of the $ZrTe_5$ electronic band structure along the k_a direction, collecting ARPES data between 16 K and 300 K. Three representative temperatures have been considered here, $T_1 = 16$ K, $T_2 = 150$ K and $T_3 = 300$ K, shown in Fig. 4(a)–(c), respectively. Fig. 4(d)–(f) shows the differential band dispersions resulting from the subtraction of the ARPES data as follow: (d) $T_3 - T_2$, (e) $T_2 - T_1$ and (f) $T_3 - T_1$.

A remarkable transfer of spectral weight is observed in all the three differential images. By cooling the sample from 300 K to ~150 K (d), the band structure moves towards lower $E - E_F$ values, consistently with our previous results [16]. However, by lowering the sample temperature, down to ~16 K, the band shift inverts

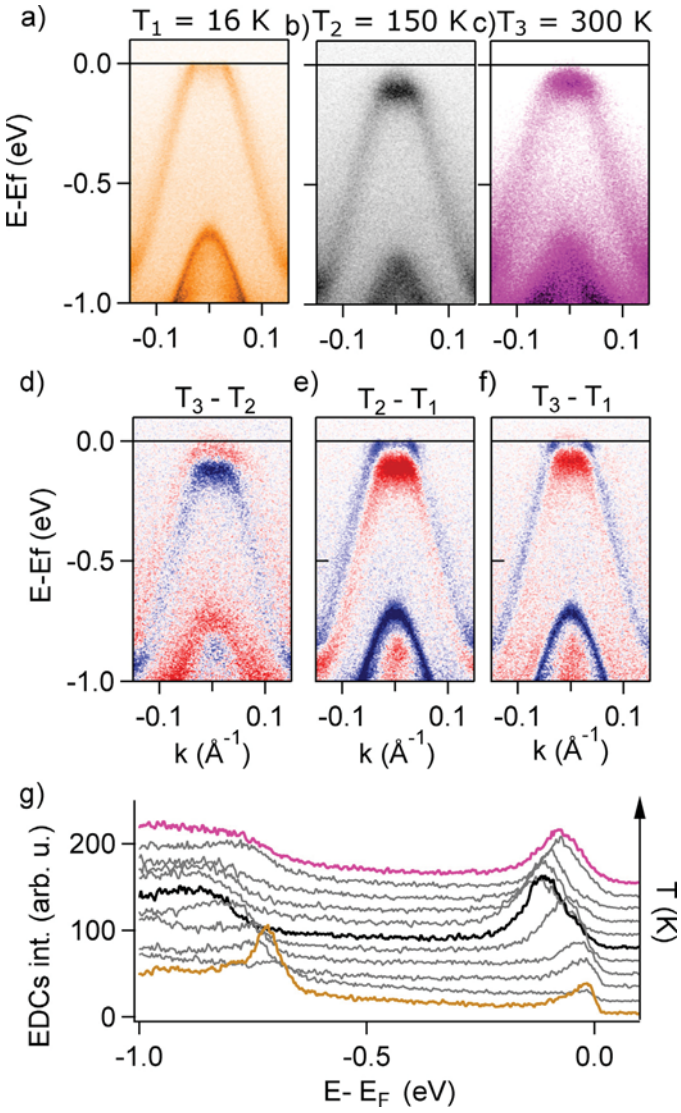

Fig. 4. (a–c) ARPES data, taken at $h\nu = 22$ eV, at (a) $T_1 = 16$ K, (b) $T_2 = 150$ K and (c) $T_3 = 300$ K. (d–f) Differential ARPES images obtained by subtracting the low temperature dispersion from the high temperature one. Blue (<0) and red (>0) features in the differential images mark the temperature driven spectral weight transfer. (g) EDC curves extracted at $k_a \simeq 0$ Å^{-1} integrating over $\simeq 0.025$ Å^{-1} from ARPES data taken at different temperatures.

direction between ∼150 K and ∼120 K unveiling a non monotonic temperature dependence.

The spectral weight transfer observed in Fig. 4(d)–(f) is interpreted as a band shift across E_F. This band shift can be better seen in Fig. 4(g) thanks to the energy distribution curves (EDCs) extracted from ARPES data taken at different temperatures between 16 K and 300 K. The EDCs have been taken at $k_a \simeq 0$ Å^{-1} and integrated over $\simeq 0.025$ Å^{-1}, the EDCs extracted from data at the three characteris-tic temperatures are shown respectively in gold (T_1), black (T_2) and violet (T_3).

A quantitative estimation of the energy shift is shown in Fig. 5(a) and it has been obtained using the following procedure. A momentum distribution curve (MDC), integrated over 20 meV, has been extracted at −0.3 eV from the ARPES measurement taken at 300 K, and the wavevectors k_a of the two peaks have been evaluated. Successively, MDCs have been extracted for all the measured tem-peratures. In these cases, the binding energies have been chosen in order to preserve the peak positions at the same wavevectors, k_a. The energy position of the MDC extracted at room temperature, $E - E_F \simeq -0.3$ eV, has been taken as reference. The reported energies shift is the difference between the MDC energy at different temperatures and the reference one.

The minimum of the shift is found at ∼150 K, hence at approximately the same temperature of the resistivity maximum, T^*. The whole trend of the energy shift, as obtained in the present study, is shown in Fig. 5 (blue squares) and it is compared to the data reported in our previous laser-ARPES work (yellow squares) [16].

The Fermi surface evolution with temperature brings complementary information about the non-monotonic band shift. In panels (b–j) of Fig. 5, we report the Fermi surfaces and different CEMs taken at $T_1 \simeq 16$ K (b–d), $T_2 \simeq 150$ K (e–g) and $T_3 \simeq 300$ K (h–j). Panels (b), (e) and (h) display the Fermi surfaces (FSs) of the material at different temperatures.

The band structure shifts toward higher binding energies, by lowering the temperature from T_3 to T^*. At T^*, the Dirac point is located at approximately E_F (Fig. 5, panel (e)). This determines a very low density of charge carriers available and the consequent rise of the resisitivity. Cooling the sample from ∼150 K to ∼16 K, the band structure shift inverts its trend, i.e. the bands move toward
lower binding energies. At T_1 the band structure reaches the largest shift value, with respect to room temperature. This observation is supported by considering that the area of the hole pocket at temperature T_1 (Fig. 5 panel (b)) is larger than the one at T_3 (Fig. 5 panel (h)). According to the raw data shown in Fig. 4(a)–(c), the band structure shift consists in a rigid change without variation of the Fermi velocity.

These findings extend our previous investigation [16], where we observed a monotonic shift of the band structure in the temperature range between 300 K and ∼125 K. By lowering further the sample temperature down to ∼16 K, we observe that the binding energy shift is clearly non-monotonic. This finding is in contrast with the data reported in Ref. [11], however it is consistent with other works [1,5] showing that at low temperature (20 K [1] and 24 K [5]) the bulk valence band (BVB) is crossing E_F and the Dirac point is unoccupied.

Although these ARPES study could justify the resisitvity peak at T^*, a simple sign reversal of the Seebeck coefficient is still unexplained by a rigid and non-monotonic band shift, as observed in the present experiments. Hence, our new data, taken on a wider temperature range then before, call for a novel and different explanation for the charge carrier sign, with respect to what we have previously proposed [16].

3.3. Topological character

In order to contribute to the debate about the topological character of $ZrTe_5$ [1–3,5,6], we present in Fig. 6 high resolution ARPES data, as measured at 16 K and at a photon energy of ∼22 eV.

Fig. 6(a) shows the Fermi surface of $ZrTe_5$, where the blue and green markers highlight the concentric hole pockets contours. These two quasi-degenerate bands crossing the Fermi Level can be easily observed in Fig. 6(b), where an ARPES image taken at $k_c = 0$Å^{-1} is shown. The presence of the two bands have been already reported in the literature [6,22] and they have been inter-preted in terms of bands with a bulk and a surface dominant character, respectively [6].

In order to provide clear evidence about the presence of two distinct states in proximity of E_F, we also analyze a momentum distribution curve (MDC), integrated over 15 meV, as shown in Fig. 6(b). The resulting MDC intensity is reported in Fig. 6(c). Each branch at both positive and negative wavevectors is clearly doubled, thus confirming the presence of two distinct states in proximity of E_F at ∼16 K.

We have shown that the h_1 band is composed by the superposition of two different states which, in another work [6], have

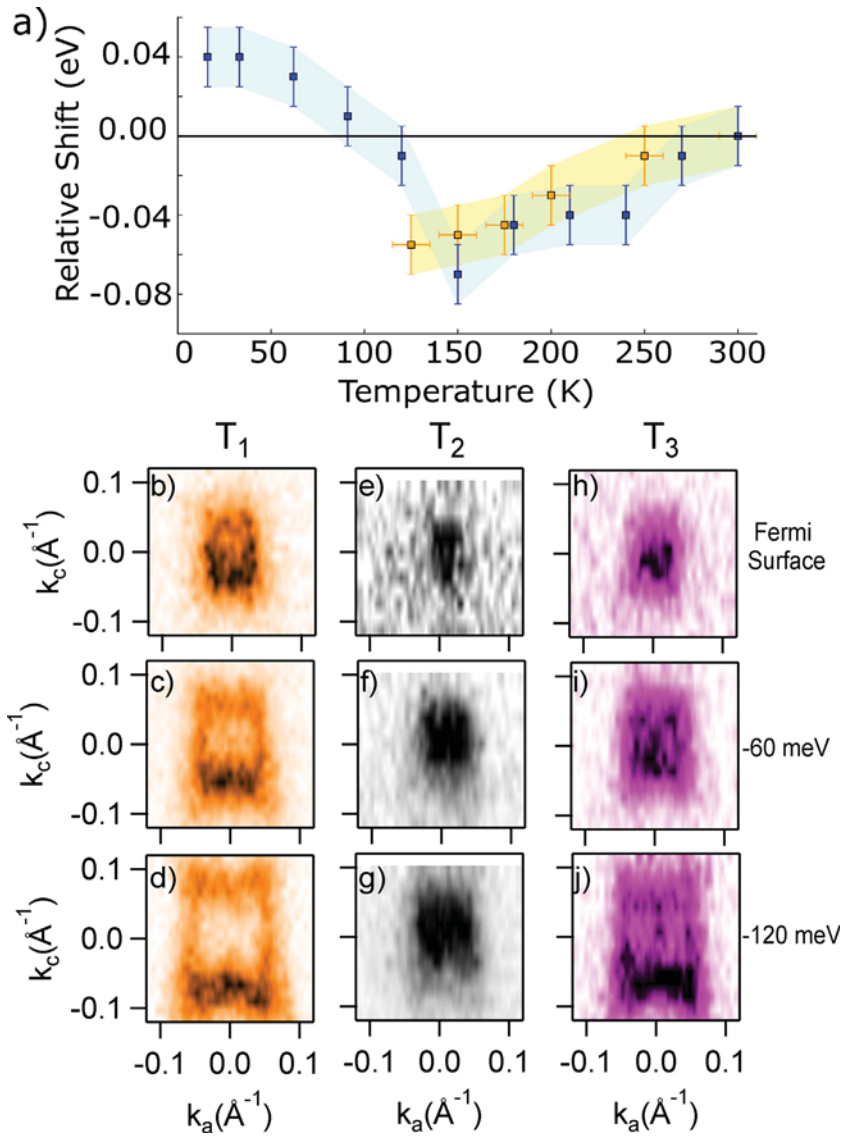

Fig. 5. (a) Evolution of the extracted energy shift as a function of the temperature (blue) compared to the one of Ref. [16] (yellow). (b–j) Constant energy maps taken at E_F, at −60 meV and at −120 meV, at three different temperatures ($T_1 \simeq 16$ K, $T_2 \simeq 150$ K and $T_3 \simeq 300$ K).

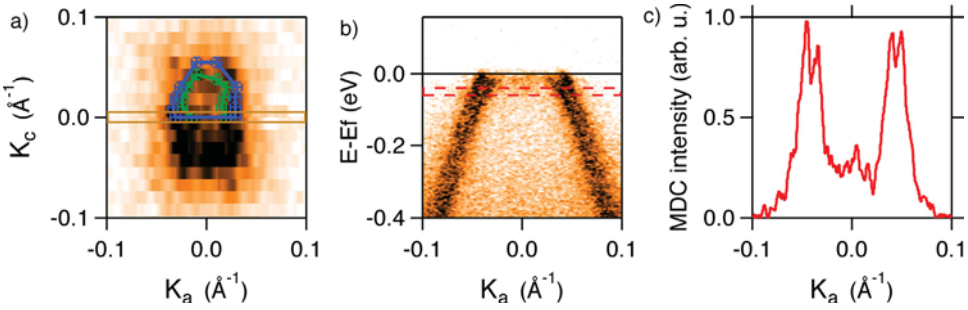

Fig. 6. (a) Fermi Surface collected at temperature 16 K and photon energy of 22 eV. The blue and green markers indicate the two concentric hole pockets position. (b) Electronic band structure at $k_c = 0$ Å^{-1}. (c) MDC extracted in proximity of E_F. The band appears to be double peaked indicating the presence of two quasi-degenerate states.

been interpreted as a surface state (SS) and a bulk valence band (BVB). The proposed existance of a SS and a BVB suggests that $ZrTe_5$ belongs to the STI phase. In the STI phase the SS is expected to be spin polarized.

The need to study the spin texture of strongly spin–orbit-coupled materials has recently promoted circular dichroic angular resolved photoelectron spectroscopy (CD-ARPES) as an indirect but powerful tool to detect the spin polarization. Although, a quantitative analysis requires to account for final state and photoelectron interference effects [23].

Fig. 7(a) reports the ARPES data measured at 22 eV, with linear horizontal polarization at ∼210 K. These data are used for comparison with the CD-ARPES data taken at ∼210 K shown in Fig. 7(b). This figure has been obtained from the difference $I^L - I^R$ between

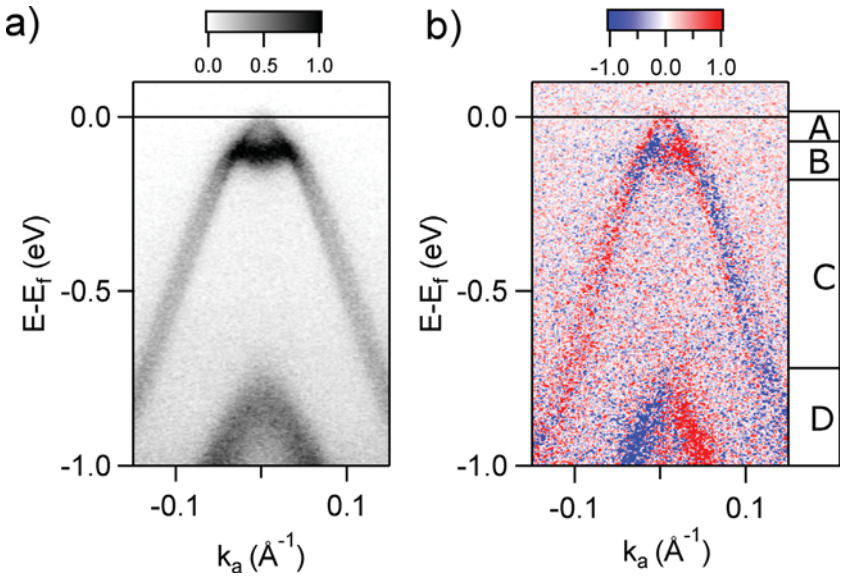

Fig. 7. (a) ARPES image taken at $h\nu = 22$ eV and $T = 210$ K. The photon energy was linear horizontal. (b) Dichroic differential image obtained from the difference $I^L - I^R$ where I^L and I^R have been obtained with circular polarized light (left and right, respectively). The image has been divided in four energy regions of interest *A*, *B*, *C* and *D*.

the two ARPES data obtained with left (I^L) and right (I^R) circularly polarized light.

Fig. 7(b) can be divided in four different energetic regions. In region *A*, *B* and *C* the SS and the BVB have been taken in exam. In particular, *A* and *C* present the same behaviour, i.e. positive signal for negative k_a and vice versa. Important is to note that in the region *A* the BVB and the SS states are well separated in energy, whereas they are almost degenerate in the region *C*.

Region *B* presents an opposite behaviour. The signal is negative for negative values of k_a and vice versa. In this region the CD signal is clearly distributed along the M-like shape of BVB, thus resulting mainly from the bulk state.

In a STI, the existence of a topologically protected surface state is a consequence of an inversion in the energy ordering of the states forming the band gap. These are also characterized by different parities at time reversal invariant high symmetry points (in particular, in the present case at Γ) [24]. In the case of $ZrTe_5$, the opening of an inverted band gap has been also interpreted as the origin of the *M*-like shape at the BVB top. We propose that the CD signal sign reversal at the top of BVB might be the signature of this band inversion between the bottom of the CB and the top of the BVB.

Finally, in the region *D*, the h_2 band presents a very strong dichroic signal. This band exhibits an opposite character, compared to the behavior of the BVB and the SS in region *C*. This confirms that h_2 is not a replica of the BVB. Hence, the CD ARPES signal indi-cates a different orbital character of h_2 compared to the BVB and, eventually, about the different spin texture, compared to the SS.

4. Conclusions

In the present work, we have performed high resolution ARPES measurements and core level analysis on $ZrTe_5$.

We have observed a doubling of the 4*d* Te core levels which, on the basis of DFT calculations, has been attributed to the chemical shift due to the presence of non-equivalent Te atoms in the crystal surface.

Our ARPES results show a temperature evolution of the $ZrTe_5$ band structure, revealing a non-monotonic energy shift of the states across the Fermi Level. This energy band shift reaches its minimum at $\sim T^*$. These findings could explain the resistivity anomaly of $ZrTe_5$. Unfortunately, the non-monotonic character of the binding energy shift of the Dirac cone reopens the question about the sign reversal of the Seebeck coefficient.

High resolution ARPES measurements reveal the presence of two quasi-degenerate bands, forming the h_1 state, crossing the Fermi level at very low temperature, 16 K. The band structure present also a band, h_2, with Fermi velocity comparable to h_1. The two bands h_1 and h_2 reveal a strong and opposite dichroic signal and the associated CEMs show that they have very different constant energy contours. In particular, h_2 displays a one-dimensional character, with little dispersion along k_c.

CD ARPES measurements bring novel information about the band inversion at the top of the valence band. The strong dichroic signal detected in proximity of E_F has been interpreted as the indication of the presence of spin polarized states, as also recently observed in spin resolved ARPES measurements [25], suggesting that $ZrTe_5$ is a strong topological insulator.

Acknowledgments

We acknowledge G. Miceli for helpful discussions about the computation of core-level shifts within the DFT framework. We also acknowledge F. Giusti for the graphical support. This work was supported in part by the Italian Ministry of University and Research under Grant Nos. FIRBRBAP045JF2 and FIRB-RBAP06AWK3 and by the European Community Research Infrastructure Action under the FP6 Structuring the European Research Area Program through the Integrated Infrastructure Initiative Integrating Activity on Synchrotron and Free Electron Laser Science, Contract No. RII3-CT-2004-506008. G.A. and O.V.Y. acknowledge support by the NCCR Marvel and the ERC Starting grant TopoMat (Grant No. 306504). A.A. acknowledges funding from the Ambizione fellowship of the Swiss SNF. First principles calculations have been performed at the Swiss National Supercomputing Centre (CSCS) under project s675.

References

[1] Q. Li, et al., Nat. Phys. (2016).
[2] R.Y. Chen, et al., Phys. Rev. Lett. 115 (2015) 176404.
[3] H. Weng, et al., Phys. Rev. X 4 (2014) 011002.
[4] X.-B. Li et al., arXiv:1601.05930v1, 2016.
[5] R. Wu et al., arXiv:1601.07056v1, 2016.
[6] G. Manzoni et al., arXiv:1608.03433, 2016.
[7] E.F. Skelton, et al., Solid State Commun. 4 (1982) 1.

[8] T.E. Jones, et al., Solid State Commun. 42 (1982) 793.
[9] M. Izumi, et al., Solid State Commun. 42 (1982) 773.
[10] M. Rubinstein, Phys. Rev. B 60 (1999) 1627.
[11] F.J. DiSalvo, et al., Phys. Rev. B 24 (1981) 2935.
[12] Y. Zhang et al., arXiV:1602.03576v1 (2016).
[13] G.N. Kamm, et al., Phys. Rev. B 31 (1985) 12.
[14] S. Okada, et al., J. Phys. Soc. Jpn. 49 (1980) 839.
[15] S. Okada, et al., J. Phys. Soc. Jpn. 51 (1982) 460.
[16] G. Manzoni, et al., Phys. Rev. lett. 115 (2015) 207402.
[17] F. Lévy, H. Berger, Journal of Crystal Growth 61 (1983) 61.
[18] H. Fjellvag, A. Kjejshus, Solid State Commun. 60 (1986) 91.
[19] P. Giannozzi, et al., J. Phys.: Condens. Matter 21 (2009) 395502.
[20] A. Crepaldi, et al., Phys. Rev. Lett. 109 (2012) 096803.
[21] A. Pasquarello, M.S. Hybertsen, R. CAr, Phys. Rev. Lett. 74 (1995) 1024.
[22] D.N. McIlroy, et al., J. Phys.: Condens. Matter 16 (2004) L359.
[23] A. Crepaldi, et al., Phys. Rev. B 89 (12) (2014) 125408.
[24] M.Z. Hasan, C.L. Kane, Rev. Mod. Phys. 82 (2010) 3046.
[25] G. Manzoni et al., 2016, in preparation.